Electronic Supplementary Information to the manuscript: Dynamics of a plasmon-activated p-mercaptobenzoic acid layer deposited over Au nanoparticles using time-resolved SERS

Gina Smith,‡ Jean-Sébastien Girardon, Jean-François Paul and Elise Berrier *

Univ. Lille, CNRS, Centrale Lille, ENSCL, Univ. Artois, UMR 8181 - UCCS - Unité de Catalyse et Chimie du Solide, F-59000 Lille, France.
‡ Present address: School of Chemistry, University of Edinburgh, Joseph Black Building, David Brewster Road, Edinburgh, Scotland EH9 3JJ.

* Elise.Berrier@univ-lille1.fr

Contents

---

1 Picture of the coffee-ring pattern

A micrograph of the analysed zone is presented in Figure S1. Micron-sized aggregated of Au-containing deposit are clearly visible along the contour of the coffee-ring pattern obtained after deposition and drying processes.

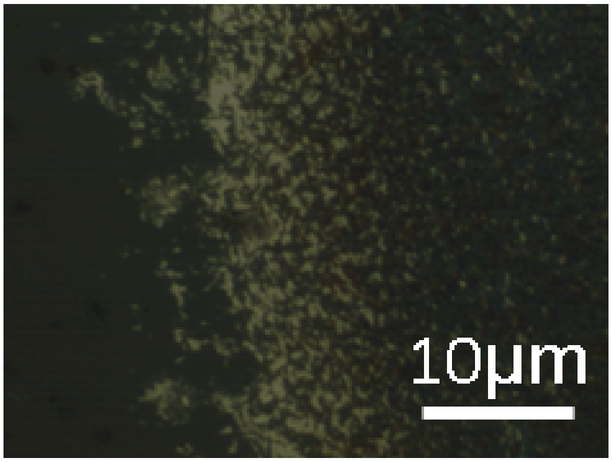

Figure S1 100X picture of the contour of the drop-coating deposit from a mixture of p-MBA and Au-citrate colloids

2 Conventional Raman spectra of commercial p-MBA powder and SERS of p-MBA:AuNPs

The conventional Raman spectra of the commercial p-MBA and the SERS fingerprint of the deposit of p-MBA+Au are presented in Figure S2. It is to be noticed that the contour line of a coffee-ring pattern prepared without AuNPs gave no detectable Raman signal.

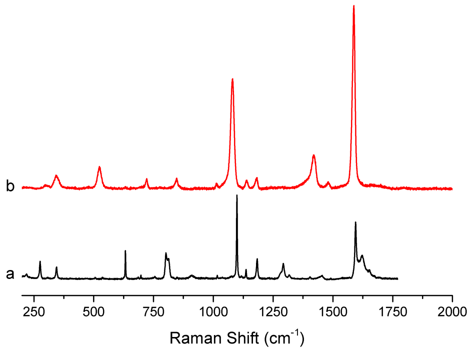

Figure S2 Conventional Raman spectrum of powder p-MBA (a) and SERS features of the drop-coating deposit of the mixture MBA+Au colloids

Both spectra are in quite good agreement with results reported for the very same system. The experimental observed wavenumbers together with a review of assignments gathered from the literature are presented in Table S1.

Raman Shift	(cm^{-1})	Assignment	Symmetry
p-MBA	pMBA:Au	(Wilson notation)	
633 (0,16)	632	ν_{6b}	B_2
686 (0,01)	693	ν_{6a}	A_1
698 (0,02)	693	$\delta(CO_2)$	
755 (0,03)	720	ν_4	B_1
802 (0,43)		$\delta(CO_2)$ in COOH	
813 (0,32)		$\nu(17b)$;	B_1
847 (0,02)	848	ν_{10b}	B_1
	860 (sh)	$\delta(CO_2)$ in COO^-)	
911 (0,1)		$\delta(CSH)$	B_2
970 (0,03)		ν_{17a}	A_2
1017 (0,03)	1012	ν_1	A_1
1038 (0,02)		ν_{18a}	A_1
1099 (0.75)	1078	ν_{12}	A_1
1117 (0,04)		$\gamma(OH)$	
1136 (0,08)	1142	ν_{18b}	B_2
1183 (0,26)	1179	ν_{9a}	A_1
1281 (sh)	1248 (vw)	ν_3	B_2
1293 (0,4)	1290 (vw)	ν_{14}	B_2
1310 (sh)		$\delta(OH); \nu(C-\phi)$	B_2
1317 (0,07)			
1404 (0,02)	1380 (sh)		
	1422	$\nu_s(COO^-)$	
1444 (sh)		ν_{19b}	B_2
1454 (0,09)	1480 (vw)	ν_{19a}	A_1
1569 (0,02)	1564 (vw)	ν_{8b}	B_2
1595 (1)	1587	ν_{8a}	A_1
1623 (0.9)		$\nu_s(C=O)$	A_1
1653 (0,3)		$\nu_s(-C=O)$	A_1

Table S1 Experimental wavenumbers and assignments of powdered p-MBA and MBA+Au compounds; in brackets: relative contribution of the Raman peak with regards to the main peak observed at 1595cm^{-1}; sh: shoulder, vw: very weak; br: broad δ:bending, γ:rocking, ν:stretching

3 SERS spectra of the series recorded at various P_S

3.1 Specific power at the sample: $5.5 \times 10^3\,\mathrm{W\,cm^{-2}}$, acquisition time: $5\,\mathrm{s}$

Because the laser power at the sample is quite low, an acquisition time of 5 seconds was applied for improving the spectral quality. One Raman spectrum was recorded every 10 s, so that a rest time of 5 s without laser exposure was applied. Under these conditions, the SERS feature of the analyte remains remarkably stable with time, as can be seen from Figure S3.

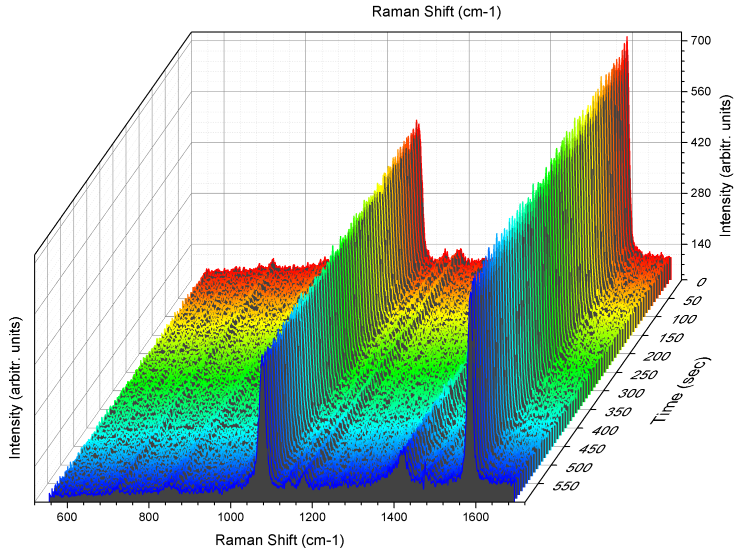

Figure S3 600-1700 $\mathrm{cm^{-1}}$ SERS features of MBA+Au as a function of time, acquisition time: $5\,\mathrm{s}$, time interval between 2 spectra: $10\,\mathrm{s}$; laser shutter kept closed between 2 acquisitions

The spectral area was found to gently decrease with time. Few discrepancies have been highlighted by a in depth descriptive statistics study, which are all assigned to either a spectral artifact or a slight change in the baseline intensity.

3.2 Specific power at the sample: $5.5 \times 10^4\,\mathrm{W\,cm^{-2}}$, acquisition time:0.5s

A slight power increase made it possible to shortens the spectral acquisition time to 0.5s and, thus, increase the frequency of spectral acquisition. Consequently, SERS spectra of 500ms were recorded every second for ca. 9 minutes. The SERS intensities obtained using an acquisition interval of 1 s are presented in Figure S4 in the form of a contour plot. The map coordinates are the spectrum number (equivalent to time, horizontal) and wavenumber (vertical) while the colors reflects the SERS intensity from dark blue (low) to red (high).

In the temporal map presented in Figure S4, the continuous horizontal lines are consistent with the main peaks of MBA:AuNPs SERS, namely observed at 1587, 1078, 1421 $\mathrm{cm^{-1}}$ and, at a minor extend, 1480, 1178, and 1143 $\mathrm{cm^{-1}}$. Isolated spots are also detected and highlighted by wite arrows in Figure S4. In particular, the spectra recorded at 157 and 197 s individually feature original profile, which look fully reversible. Non-reversible changes also occurred: the intensities of both Raman peaks detected at 997 and 1021 $\mathrm{cm^{-1}}$, pointed out by horizontal green arrows in Figure S4, as well as the contribution at 1570 $\mathrm{cm^{-1}}$ irreversibly increased with time.

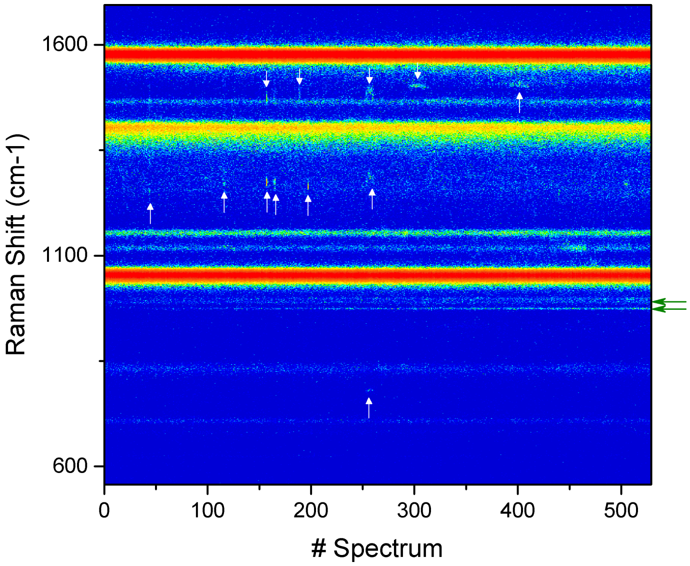

Figure S4 Contour plot of normalized SER spectra of MBA:Au deposit; $P_S = 5.5 \times 10^4\,\mathrm{W\,cm^{-2}}$; acquisition time:$0.5\,\mathrm{s}$, interval:$1\,\mathrm{s}$

3.3 Specific power: $5.5 \times 10^4\,\mathrm{W\,cm^{-2}}$, acquisition time: $0.5\,\mathrm{s}$

The experiment run at P_S=$5.5 \times 10^4\,\mathrm{W\,cm^{-2}}$ was largely discussed in the manuscript. We propose here a specific investigation of the main *individual event* observed during the Series. Figure S5 shows the raw spectra, without any baseline correction nor intensity normalization, recorded at t=156, 157 and 158s. By comparing the baseline intensity of the three spectra, it is clear that the individual event observed at t=157s is not correlated to an enhancement of the background signal intensity. The spectral difference between the lines recorded at 157 and 156s clarify that only two modes are specifically enhanced at t=157s, which are visible at 1296 and 1491 $\mathrm{cm^{-1}}$. This trend is typical of chemical enhancement (CE).

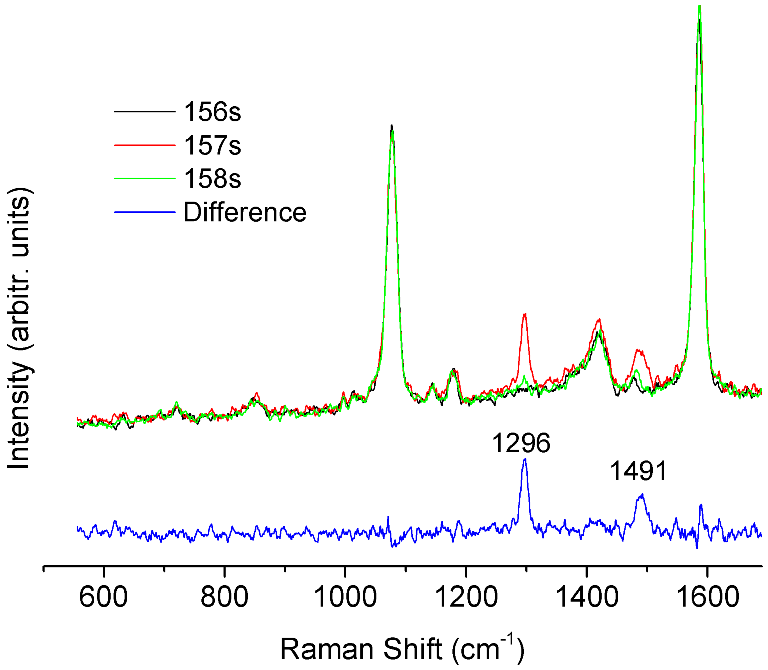

Figure S5 As recorded SER spectra of p-MBA:AuNPs recorded at t=156, 157 and 158s ; P_S=$5.5 \times 10^4\,\mathrm{W\,cm^{-2}}$, acquisition time: $0.5\,\mathrm{s}$, time interval between 2 spectra: $1\,\mathrm{s}$; laser shutter kept closed between 2 acquisitions

3.4 Specific power: $2.3 \times 10^5\,\mathrm{W\,cm^{-2}}$, acquisition time: $0.5\,\mathrm{s}$

The evolution with time of the spectral area is presented in Figure S6. Exceptionally high or low area values are reported with red and green scatters, respectively.

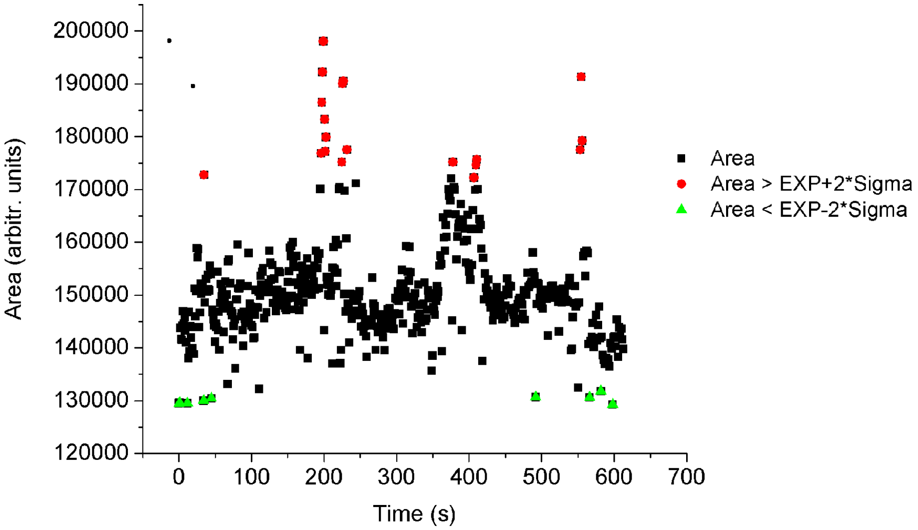

Figure S6 Area of SER spectra of MBA:Au deposit as a function of time; P_S=$2.3 \times 10^5\,\mathrm{W\,cm^{-2}}$; acquisition time:$0.5\,\mathrm{s}$, interval:$1\,\mathrm{s}$

In the following are presented 3 Series which were successively recorded over the same region of the sample. The laser specific power at the sample was set to $2.3 \times 10^5\,\mathrm{W\,cm^{-2}}$ upon spectral acquisition. Three series of SERS acquisition were successively run over the same region of the sample. Between each series, a "rest" time of 10 minutes in the dark was observed.
The acquisition time was 500 ms and one acquisition was programmed every second.
The first Series presented here is consistent with the results presented in the manuscript for P_S=$2.3 \times 10^5\,\mathrm{W\,cm^{-2}}$.

3.4.1 Waterfall presentation

During the first 2 Series, the SERS signal was subjected to strong fluctuations without producing dramatic non-reversible changes. On the other hand, the SER spectrum p-MBA layer was found to be significantly altered at the end of the third Series (Figure S7c).

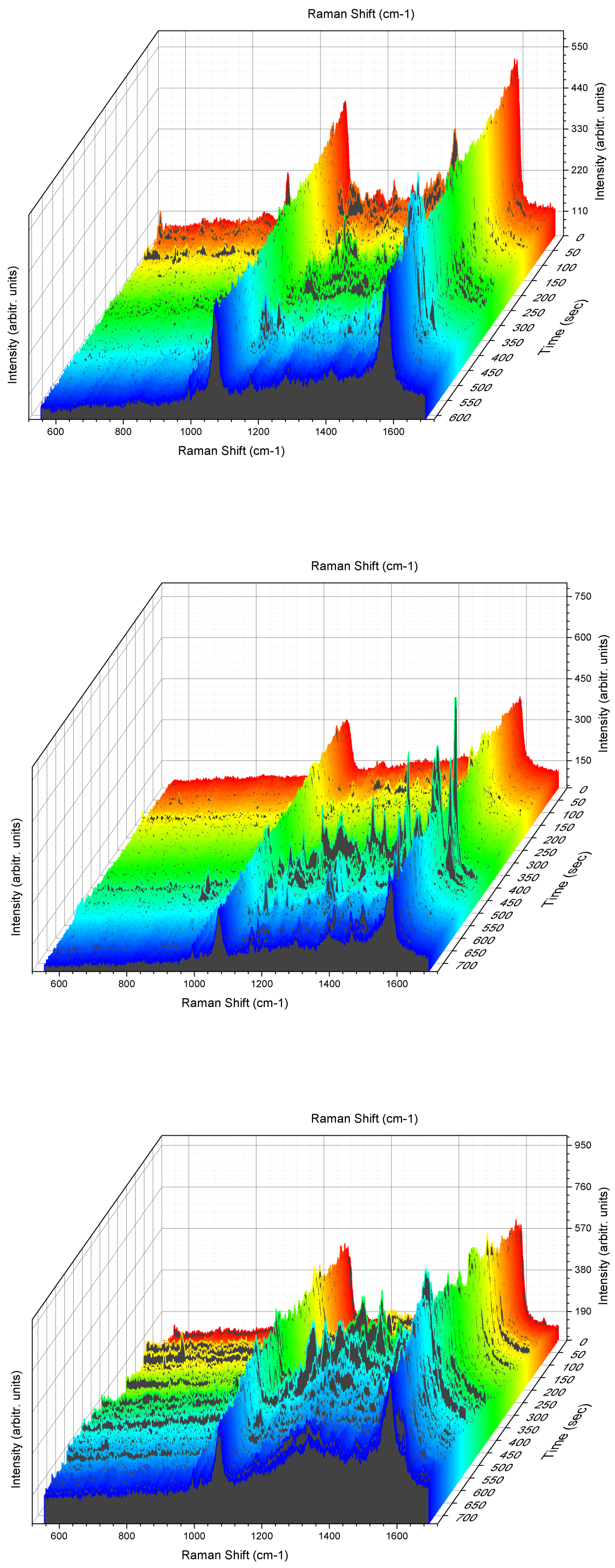

Figure S7 SERS spectra recorded over the same point of sample along three successive series using a laser specific power of $2.3 \times 10^5\,\mathrm{W\,cm^{-2}}$ at the sample. 1 spectra was acquired every second; acquisition time: $0.5\,\mathrm{s}$, laser shutter kept closed between 2 acquisitions; the sample was kept 10 minutes without laser exposure between 2 series

3.4.2 Contour plot

In this section are presented 3 Series presented in the previous section in the form of a contour plot. The mapping coordinates are the spectrum number, which correspond to 1 second of time(horizontal axis) and the Raman shift (vertical axis).

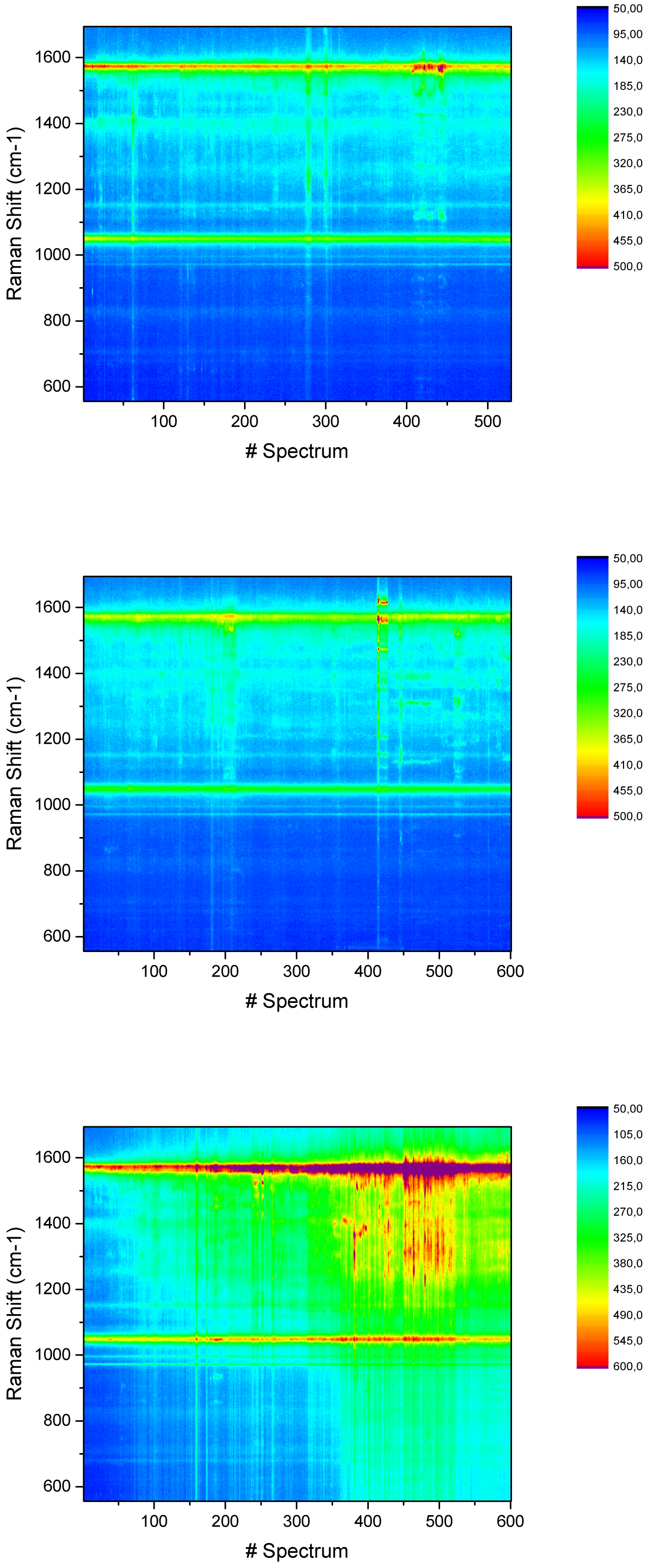

Figure S8 Contour plot of SERS features obtained during the 3 Series recorded using a laser specific power of $2.3 \times 10^{5}\,\mathrm{W\,cm^{-2}}$ at the sample. 1 spectra was acquired every second; acquisition time: $0.5\,\mathrm{s}$, laser shutter kept closed between 2 acquisitions; the sample was kept 10 minutes without laser exposure between 2 series

Both waterfall and contour plot presentations suggest that the non-reversible changes are minor during the two first Series whereas the third one exhibits clear sample degradation and the formation of polyaromatic hydrocarbons (PAHs). Still, the individual events are remarkable, owing to their frequency of occurrence and relative intensity during the two first Series.

3.5 Covariance plot of the first Series recorded with P_S=2.3 × 10^5 W cm^{-2}

In order to have a global picture of the way the spectral trends evolve, either in a synchronized manner or not, we have calculated the covariance matrix built with the covariance values $\sigma(\bar{\nu_n},\bar{\nu_m})$ crossing the the intensities $I_i(\bar{\nu_n})$ and $I_i(\bar{\nu_m})$ of the SERS signal recorded at $t = i$ for the two wavenumbers $\bar{\nu_n}$ and $\bar{\nu_m}$, respectively.

$$\sigma(\bar{\nu_n},\bar{\nu_m}) = \frac{1}{N}\sum_i [(I_i(\bar{\nu_n}) - \langle I(\bar{\nu_n})\rangle) \times (I_i(\bar{\nu_m}) - \langle I(\bar{\nu_m})\rangle)] \qquad (1)$$

$\langle I(\bar{\nu_n})\rangle$ and $\langle I(\bar{\nu_m})\rangle$ are the expected values of the SERS intensity at $\bar{\nu_n}$ and $\bar{\nu_m}$, respectively.

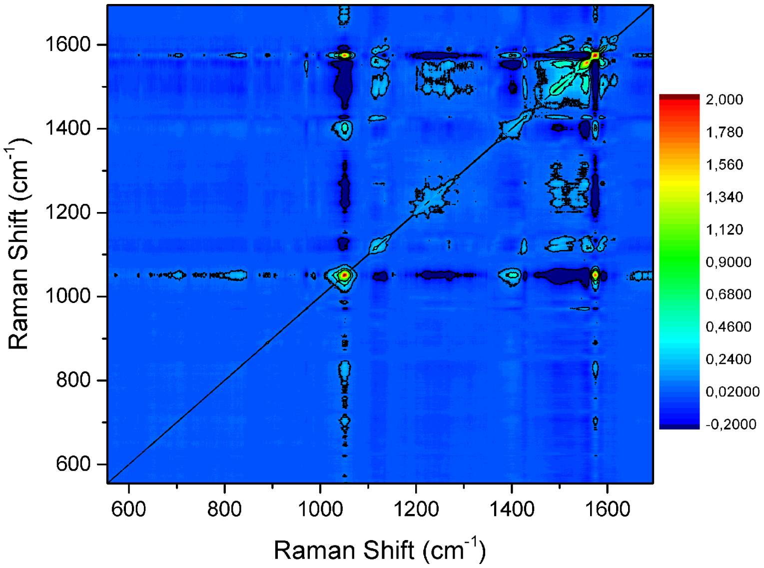

Figure S9 Covariance map of intensity fluctuations . The spectral intensities were normalized by the area of each spectrum. P_S=2.3 × 10^5 W cm^{-2}

The covariance map is particularly relevant in refining the evolutions of peaks whose wavenumbers are close to each other. On average, the covariance map is in good agreement with the one of the experiment run at P_S=5.5 × 10^4 W cm^{-2} presented in the manuscript, even though the spots are better defined. A careful analysis of the spectral correlations by means of the covariance values made it possible to highlight two groups of peaks which are not related to non-reversible processes such as decarboxylation and which occur competitively. The first group, further denoted as Group I is composed by noticeable signals 716, 1078, 1422 and 1587 cm^{-1} while the second one (Group II) gathers lines at at 632, 1142, 1248, 1290, 1444 and 1515 cm^{-1}. A tentative assignment based on the normal modes of substituted benzene and comparison with literature data is presented in Table S2.

The SER spectra showing the so-called *individual events* responsible of high Kurtosis values, as presented in the manuscript, are presented in Figure S10.

Figure S10 shows the most spectacular spectral peculiarities in regions already highlighted by means of the Kurtosis descriptor. Recurrent peaks or group of peaks with variable intensities are also detected in spectral regions around 945-960 cm^{-1}, 1130-1180 cm^{-1}, 1240-1290 cm^{-1}, 1435-1445 cm^{-1} and 1500-1520 cm^{-1}. An individual peak is also observed at 1620 cm^{-1} at t=420 s (Figure S10f). The Raman spectrum obtained at t=12 s is unique, featuring lines at 910 (medium), 1032, 1281, 1414 and 1446 cm^{-1}. The Raman line detected around 910 cm^{-1} can plausibly be assigned to the $\delta(CSH)$ bending mode and the other exceptional lines are consistent with characteristic modes of free p-mercaptobenzoate species (Table S1). The adsorption energy of p-MBA on gold surfaces is high enough to prevent the observation of a thiol group in the immediate vicinity of the gold nanostructure using an acquisition time of 0.5 s^6. Therefore, we propose that in this precise case, the signal comes from the second monolayer of p-MBA.

Raman Shift (cm^{-1})	Assignment	Symmetry (C_2v)	Approximative description	Ref.
Group I				
721	4	B_1	out of plane ring puckering	1
1078	12	A_1	in plane CCC bending	1–3
1422	$\nu_s(COO^-)$	B_1		1–3
1587	8a	A_1	in plane ring CC stretching	1–3
Group II				
632	6b	B_2	in plane CCC bending	4
1142	18b	B_2	in plane CH bending	3
1248	3	B_2	in plane CH bending	
1290	14	B_2	in plane CH bending, CC stretching	3
1444	19b	B_2	in plane CC stretching, CH bending	
1564	8b	B_2	in plane ring CC stretching	5

Table S2 Assignment of Group I and Group II peaks; the vibrations related to the normal modes of substituted benzene are presented according to the Wilson notation

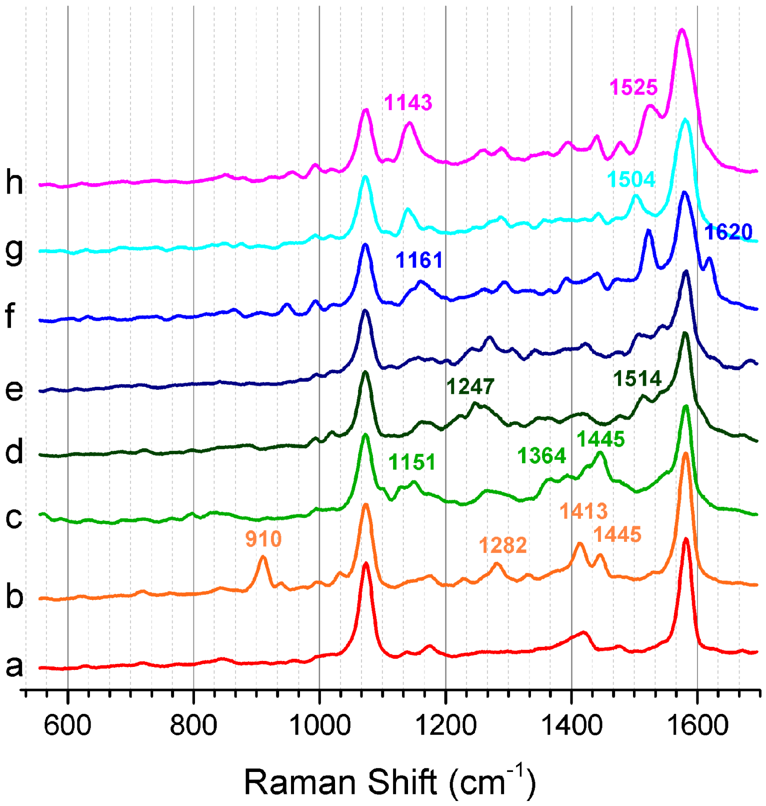

Figure S10 Selection of the most original SERS spectra recorded with P_S=$2.3 \times 10^5\,W\,cm^{-2}$ associated with the main so-called individual events recorded at a)1s (reference), b) 12s, c) 63s, d) 280s, e)300s, f)420s, g) 429s and h) 444s

4 Maximal values of Kurtosis coefficient as a function of the specific power

In line with the number of exceptionnaly high Kurtosis values, the highest Kurtosis value calculated from the Series recorded at different specific powers follows a non-linear dependence on P_S, as is shown in Figure S11.

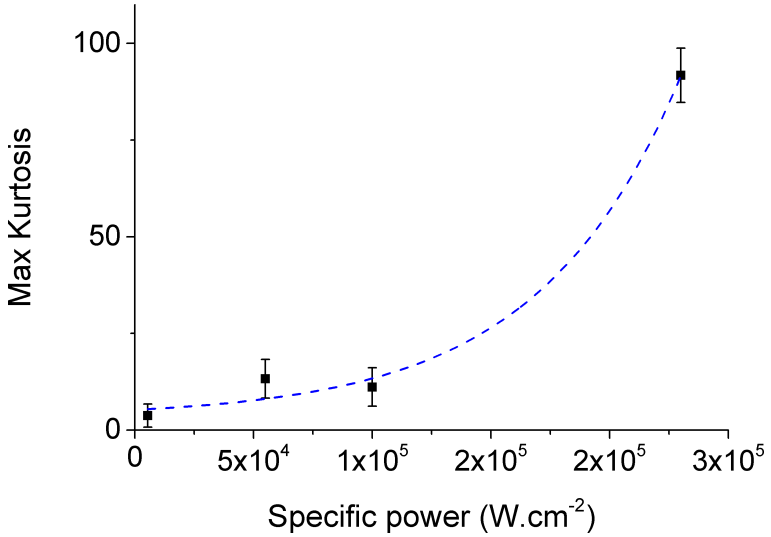

Figure S11 Maximal γ_2 values over SER spectra recorded during 10 minutes as a function of the specific power applied

This observation demonstrate that not only the number but the relative intensity of *individual events* as well is to be correlated to the laser power applied.

Acknowledgements

We thank the University of Edinburgh for supporting the 1-year research stay of Gina Smith at UCCS. Pr. Pierre Suret is acknowledged for discussions about the statistical description of extreme events.

References

[1] A. Michota and J. Bukowska, *J. Raman Spectrosc.*, 2003, **34**, 21–25.

[2] C.-H. Ho and S. Lee, *Colloids Surf. A*, 2015, **474**, 29 – 35.

[3] K. L. Nagashree, R. Lavanya, C. Kavitha, N. S. Venkata Narayanan and S. Sampath, *RSC Adv.*, 2013, **3**, 8356–8364.

[4] R. Li, H. Lv, X. Zhang, P. Liu, L. Chen, J. Cheng and B. Zhao, *Spectrochim. Acta A*, 2015, **148**, 369 – 374.

[5] M. Osawa, N. Matsuda, K. Yoshii and I. Uchida, *J. Phys. Chem.*, 1994, **98**, 12702–12707.

[6] J. V. Maya Girón, E. Zelaya, A. Rubert, G. Benítez, P. Carro, R. C. Salvarezza and M. E. Vela, *J. Phys. Chem. C*, 2013, **117**, 24967–24974.